

Is the Valence Bond Solid state in J_1 - J_2 Square Lattice Heisenberg Model Plaquette or Columnar?

Jiale Huang,¹ Xiangjian Qian,¹ and Mingpu Qin^{1,2,*}

¹*Key Laboratory of Artificial Structures and Quantum Control (Ministry of Education), School of Physics and Astronomy, Shanghai Jiao Tong University, Shanghai 200240, China*

²*Hefei National Laboratory, Hefei 230088, China*

We utilize Density Matrix Renormalization Group (DMRG) and Fully Augmented Matrix Product States (FAMPS) methods to investigate the Valence Bond Solid (VBS) phase in the J_1 - J_2 square lattice Heisenberg model. To differentiate between the Columnar Valence Bond Solid (CVBS) and Plaquette Valence Bond Solid (PVBS) phases, we introduce an anisotropy Δ_y in the nearest neighboring coupling in the y -direction, aiming at detecting the possible spontaneous rotational symmetry breaking in the VBS phase. In the calculations, we push the bond dimension to as large as $D = 25000$ in FAMPS, simulating systems at a maximum size of 14×14 . With a careful extrapolation of the truncation errors and appropriate finite-size scaling, followed by finite Δ_y scaling analysis of the VBS dimer order parameters, we identify the VBS phase as a PVBS type, meaning there is no spontaneous rotational symmetry breaking in the VBS phase. This study not only resolves the long-standing issue of the characterization of the VBS order in the J_1 - J_2 square lattice Heisenberg model but also highlights the capabilities of FAMPS in the study of two-dimensional quantum many-body systems.

I. INTRODUCTION

The J_1 - J_2 spin-1/2 square lattice Heisenberg model stands as one of the most extensively researched paradigms for studying the frustration effect in quantum many-body systems. The competing antiferromagnetic interactions between the nearest and next-nearest neighbors give rise to a rich variety of phases, which makes this model a well-known playground for searching exotic quantum states, such as Quantum Spin Liquid (QSL) and Valence Bond Solid (VBS) [1–4]. Understanding these exotic states may be crucial for elucidating the underlying physics of high-temperature superconductors and other strongly correlated materials [4–7].

Over the past few decades, extensive research has been conducted to investigate the phase diagram of the J_1 - J_2 square lattice Heisenberg model. A general agreement has been established that when $J_2 \rightarrow 0$, the model's ground state manifests as a Néel antiferromagnetic order [8], which extends to a finite region of $J_2/J_1 \approx 0.5$. For very large but finite values of J_2/J_1 , the model's ground state has antiferromagnetic (AFM) stripe order [1, 9]. Intriguingly, the intermediate regime of $0.5 \lesssim J_2/J_1 \lesssim 0.6$ is termed the non-magnetic phase, which has been a focal point of ongoing research. Many methods have been employed to study this model, including the exact diagonalization [1, 10–13], series expansion [14–16], quantum Monte Carlo [9, 17, 18], and tensor network methods [2, 19–25].

Despite the valuable insights gained from these results, which have significantly enhanced our understanding of the phase diagram of the J_1 - J_2 square lattice Heisenberg model, the nature of the non-magnetic regime

continues to be a subject of active discussion. A variety of competing states have been suggested for this regime with different methods. These potential states encompass the plaquette valence bond solid (PVBS) [2, 13, 18, 20, 24, 26–31], columnar valence bond solid (CVBS) [1, 4, 11, 15, 21, 32], and quantum spin liquid states [3, 9, 17, 18, 20, 24, 25, 33–35]. The source of these controversies can be attributed to the difficulty of accurately simulating large-scale quantum many-body systems.

Recently, a novel approach, termed Fully Augmented Matrix Product States (FAMPS), has been developed to address and mitigate the limitations inherent in the Density Matrix Renormalization Group (DMRG) method when applied to the study of two-dimensional systems [36]. This method has been subsequently applied to investigate the phase diagram of J_1 - J_2 square lattice Heisenberg model [37]. In [37], it is found that a VBS phase directly connects Néel and stripe AFM phases, indicating the absence of a spin liquid phase in the J_1 - J_2 square lattice Heisenberg model (see Fig. 1 (b)). However, the exact nature of the VBS phase, whether it is a PVBS or a CVBS, remains undetermined. To address this long-standing issue, we employ the DMRG and FAMPS methods, to investigate the nature of the VBS phase at $J_2 = 0.57$, which is deep in the VBS phase.

By applying an anisotropy Δ_y in the nearest neighboring coupling in the y -direction in the J_1 - J_2 square lattice Heisenberg model, we can detect the possible spontaneous rotational symmetry breaking of the VBS phase, which can help us to distinguish CVBS from PVBS. We push the bond dimension to $D = 25000$ in our FAMPS calculations and simulate systems with a maximum size of 14×14 . Through meticulous extrapolation with truncation errors and reliable finite-size and finite Δ_y scaling analysis, we establish that the VBS phase in the J_1 - J_2 square lattice Heisenberg model is a PVBS type.

*qinmingpu@sjtu.edu.cn

The rest of this paper is structured as follows: in Sec. II, we introduce the model in which we add an anisotropy Δ_y in the nearest neighboring coupling in the y -direction to the J_1 - J_2 square lattice Heisenberg model. We also outline the methods used to study this model and demonstrate the advantage of the FAMPS method in comparison to the pure DMRG method. In Sec. III, we present the results of the VBS dimer order parameter and discuss the approach to determine the nature of the VBS phase. We conclude our work in Sec. IV.

II. MODEL AND METHODS

A. Model

The Hamiltonian of J_1 - J_2 square lattice Heisenberg model is given by

$$H = J_1 \sum_{\langle i,j \rangle} \hat{S}_i \cdot \hat{S}_j + J_2 \sum_{\langle\langle i,j \rangle\rangle} \hat{S}_i \cdot \hat{S}_j \quad (1)$$

with $\langle i,j \rangle$ denoting the nearest neighboring sites and $\langle\langle i,j \rangle\rangle$ denoting the next-nearest neighboring sites. \hat{S}_i is the spin-1/2 operator at site i and J_1 and J_2 are the nearest and next-nearest neighboring couplings, respectively.

Our study focuses on a square lattice with $L_x = L_y$ with open boundary conditions in both directions, which preserves the rotational symmetry. The ground state of the VBS phase could potentially manifest as a twofold degenerate CVBS or a genuine PVBS. It is known that there is no spontaneous symmetry breaking for systems with finite size, so it is hard to distinguish between these two states directly in finite systems. To address this issue, we introduce an anisotropy Δ_y in the y -direction of the nearest neighboring coupling to detect the possible spontaneous rotational symmetry breaking of the VBS state in the thermodynamic limit. By first extrapolating the system sizes to the thermodynamic limit, followed by the extrapolation to the zero Δ_y limit, we can determine the true nature of the VBS phase. The new Hamiltonian is given by

$$H = \sum_r J_1 \hat{S}_r \cdot \hat{S}_{r+\hat{x}} + (J_1 + \Delta_y) \hat{S}_r \cdot \hat{S}_{r+\hat{y}} + J_2 (\hat{S}_r \cdot \hat{S}_{r+\hat{x}+\hat{y}} + \hat{S}_r \cdot \hat{S}_{r+\hat{x}-\hat{y}}) \quad (2)$$

When Δ_y is set to 0, this model reduces to the J_1 - J_2 square lattice Heisenberg model. In this work, we set $J_1 = 1.0$ as the energy unit and $J_2 = 0.57$, deep in the VBS phase as shown in Fig. 1(b).

B. Method

DMRG is a powerful numerical method for studying one-dimensional and quasi-one-dimensional quantum

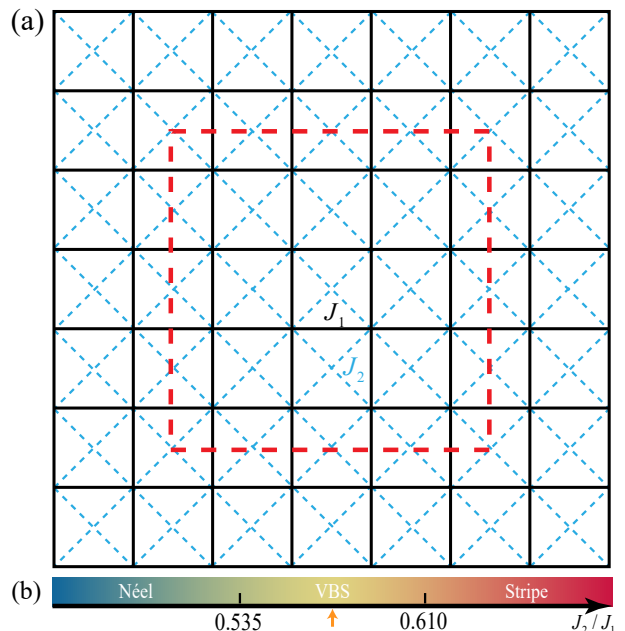


FIG. 1: (a) Illustration of an 8×8 J_1 - J_2 Heisenberg model on a square lattice, where black lines indicate nearest neighboring couplings J_1 and dashed blue lines represent next-nearest neighboring couplings J_2 . Open boundary conditions are applied in both x and y directions. The central zone marked by a red dashed area highlights the lattice region utilized for calculating the VBS dimer order parameter D_α defined in Eq. (5) (for each system, we use only the results in the central half for the calculation of D_α). (b) Phase diagram of the J_1 - J_2 square lattice Heisenberg model, illustrating a VBS phase sandwiched by the Néel and stripe AFM phases within the coupling ratio range $0.535 \lesssim J_2/J_1 \lesssim 0.610$ [37]. The orange arrow at $J_2 = 0.57$ denotes the specific coupling strength at which the VBS dimer order parameter is calculated in this work.

systems [38–40]. It is based on the Matrix Product States (MPS) ansatz which is a variational wavefunction ansatz for one-dimensional quantum systems [41–43]. The MPS ansatz is defined as

$$|\text{MPS}\rangle = \sum_{\{s_i\}} \text{Tr}(A^{s_1} A^{s_2} \cdots A^{s_N}) |s_1 s_2 \cdots s_N\rangle \quad (3)$$

where A^{s_i} is the rank-3 local tensor at site i with one physical index s_i (with dimension d) and two auxiliary indices (with bond dimension D). D is the key parameter in DMRG calculations which determines the accuracy of the calculation. Even though DMRG is designed for one-dimensional systems, it can be extended to two-dimensional systems. Nonetheless, the bond dimension required for the accurate simulation of two-dimensional systems increases exponentially with the system size, due to the area-law of entanglement entropy [44]. Hence for DMRG calculations, achieving a sufficiently large bond dimension to study a two-dimensional system with high precision becomes computationally challenging.

Recently, FAMPS method has been introduced to ad-

dress the limitations of DMRG in two-dimensional systems. This approach enhances the entanglement in MPS and improves computational accuracy by incorporating an additional layer of unitary tensors, known as disentanglers [45], to the physical indices of the MPS. The FAMPS ansatz is defined as

$$|\text{FAMPS}\rangle = D(u)|\text{MPS}\rangle \quad (4)$$

where $D(u)$ denotes the additional disentangler layer. FAMPS method has been demonstrated to attain more precise results than pure DMRG method and can support area-law-like entanglement for 2D systems while maintaining the low cost of DMRG $O(D^3)$ with a small overhead $O(d^4)$ [36, 46, 47]. In this work, we employ the FAMPS method to study the J_1 - J_2 square lattice Heisenberg model at $J_2 = 0.57$ with the largest system size 14×14 and largest bond dimension $D = 25000$. The other system sizes are studied with pure DMRG method with the largest bond dimension $D = 50000$, which gives reliable results with extrapolations with truncation errors in the DMRG calculation.

To show the improvement of FAMPS over pure DMRG method, we calculate the ground state energy per site of the J_1 - J_2 square lattice Heisenberg model at $J_2 = 0.57$ for system size $L = 14 \times 14$ under open boundary conditions (OBC). The results are presented in Fig. 2. By applying a linear extrapolation to obtain the ground state energy E_0 at the truncation errors $\varepsilon = 0$, we observe that both FAMPS and DMRG methods yield consistent results. However, the FAMPS method provides a significantly smaller error bar, indicating a more reliable and accurate estimation of E_0 . The FAMPS method achieves convergence more rapidly than the pure DMRG approach. Notably, even the data points corresponding to the largest truncation errors in FAMPS calculations align with the linear fitting line. In contrast, the data points with large truncation errors from the pure DMRG calculations deviate from the fitting line, indicating less robustness in approaching the ground state.

The convergence of the energy per site with bond dimension D is depicted in Fig. 2 (b). The results highlight that for a given bond dimension, the energy calculated using the FAMPS method consistently falls below that calculated by the pure DMRG method. Notably, the simulation accuracy of FAMPS at a specific bond dimension D is approximately equivalent to that of DMRG with bond dimension $3D$. For instance, the energy value obtained with FAMPS at $D = 15000$ is comparable to those calculated with DMRG at $D = 45000$.

III. RESULTS

The VBS dimer order parameter, denoted as D_α ($\alpha = x/y$), serves as a critical observable for distinguishing between the competing VBS states in the J_1 - J_2 square lattice Heisenberg model [35, 48]. This parameter effectively captures the possible rotational symmetry-

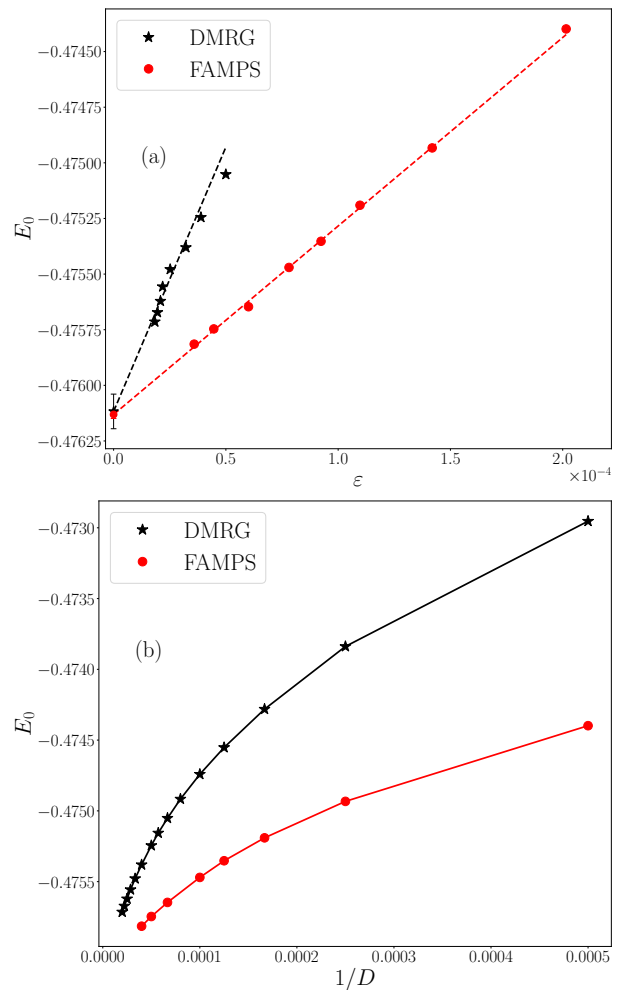


FIG. 2: (a) Ground state energy per site E_0 for the J_1 - J_2 model with $J_2 = 0.57$ and system size 14×14 under OBC, as a function of the truncation errors ε . The data is calculated using both FAMPS and pure DMRG methods. The dashed line indicates a linear fitting, which is extrapolated to $\varepsilon = 0$. Though the extrapolated results for DMRG and FAMPS are consistent, the error bar for FAMPS result is quite smaller. (b) E_0 as a function of the bond dimension D . For each D , the energy computed using FAMPS is consistently lower than that obtained with pure DMRG method. Analysis indicates that the performance of FAMPS at a given bond dimension D is approximately equivalent to pure DMRG calculation with bond dimension $3D$.

breaking, thereby providing a quantitative measure to differentiate between the CVBS and PVBS states. The definition of D_α ($\alpha = x/y$) is given by

$$D_\alpha = \frac{1}{N_b} \sum_r e^{iq_\alpha \cdot r} \hat{S}_r \cdot \hat{S}_{r+\alpha} \quad (5)$$

where N_b is the number of bonds in the calculation, q_α is the wave vector associated with the VBS order, taking values $(\pi, 0)$ or $(0, \pi)$ depending on the direction α of the dimer order. In the thermodynamic limit, for the CVBS state, either D_x or D_y will be non-zero while the other

approaches zero. Conversely, for the PVBS state, both D_x and D_y should exhibit non-zero values, and the ratio $|\langle D_x \rangle|/|\langle D_y \rangle|$ should be unity, indicating an isotropic dimer distribution across the lattice. The illustration of the PVBS and CVBS dimer is shown in Fig. 3.

In our study, by adding an anisotropy Δ_y in the nearest neighboring coupling in the y -direction to the J_1 - J_2 square lattice Heisenberg model, we can detect the possible spontaneous rotational symmetry breaking of the VBS state. As shown in Fig. 4, though the strong coupling bonds (with larger $|\langle \hat{S}_r \cdot \hat{S}_{r+\alpha} \rangle|$) form a plaquette structure, the rotational symmetry is broken due to the inclusion of the Δ_y term in Eq. (2). This rotational symmetry breaking can be detected by the VBS dimer order parameter.

In Fig. 5, we present the main results about VBS dimer order parameter D_α as a function of the anisotropy Δ_y for $J_2 = 0.57$ across various system sizes $L \times L$. To reduce the finite-size effect, we only use results in the central half of the studied systems. We can find that as Δ_y increases, D_x (D_y) decreases (increases). For $\Delta_y \gtrsim 0.2$, D_x almost approaches zero while D_y has a finite values. This behavior is consistent with theoretical expectations of Eq. (2), where rotational symmetry is explicitly broken by including the Δ_y term. We also notice that as expected, when $\Delta_y = 0$, $D_x = D_y$ for given systems, because spontaneous symmetry breaking can't occur for finite systems. To detect the possible spontaneous rotational symmetry breaking, we need to focus on how D_α behaves as Δ_y approaches zero.

To accurately determine the true VBS phase type at $\Delta_y = 0$, we have to extrapolate D_α to the thermodynamic limit $L \rightarrow \infty$. In this process, the order in which the limit is taken is critical. We first approach the thermodynamic limit and then take the limit of vanishing anisotropy Δ_y . This approach can be formally expressed as

$$D_\alpha = \lim_{\Delta_y \rightarrow 0} \lim_{L \rightarrow \infty} D_\alpha \quad (6)$$

In this study, we first perform a linear extrapolation to $L \rightarrow \infty$ for fixed Δ_y . An example for $\Delta_y = 0.03$ is shown in Fig. 6, and results for other Δ_y values are shown in Appendix. A. We subsequently apply a quadratic fitting of extrapolated D_α with Δ_y to obtain the spontaneous order parameters. The results are shown in Fig. 5.

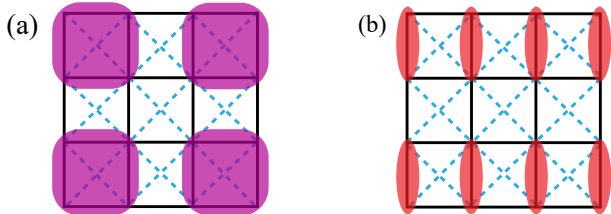


FIG. 3: (a) PVBS state with D_x equals to D_y . (b) CVBS state with D_y is non-zero and D_x is vanishing.

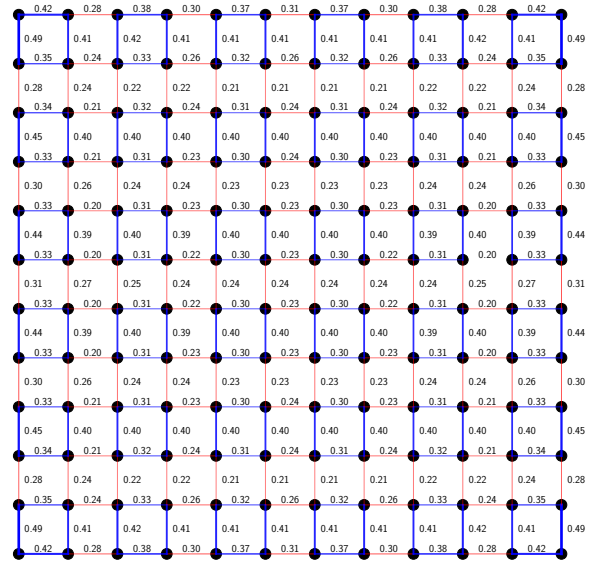


FIG. 4: The bond strength $|\langle \hat{S}_r \cdot \hat{S}_{r+\alpha} \rangle|$ of the 12×12 system at $\Delta_y = 0.03$. The blue line shows the strong coupling bonds and the red line shows the weak coupling bonds.

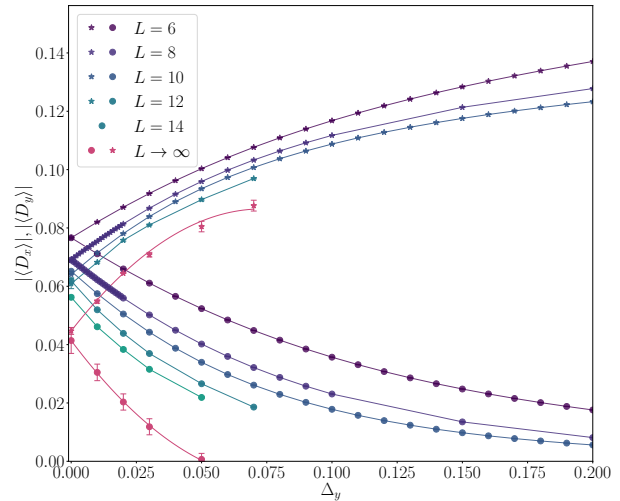


FIG. 5: The VBS dimer order parameter D_α versus Δ_y with D_y denoted as star markers and D_x denoted as circle markers. All data have been extrapolated to truncation errors $\varepsilon = 0$. The red markers represent values extrapolated to the thermodynamic limit ($L \rightarrow \infty$). Quadratic fitting is applied to these extrapolated points versus Δ_y . The convergence of fitting lines at $\Delta_y = 0$ strongly suggests that there is no spontaneous rotational symmetry breaking in the VBS phase and the VBS phase is a PVBS type.

If the VBS phase was a CVBS type, D_x would vanish and D_y remain non-zero, due to the applied anisotropy Δ_y in the y -direction of the nearest neighboring coupling. But we find that the fitting curves for D_x and D_y exhibit remarkable convergence at $\Delta_y = 0$, as depicted in Fig. 5. This convergence strongly suggests that the VBS phase

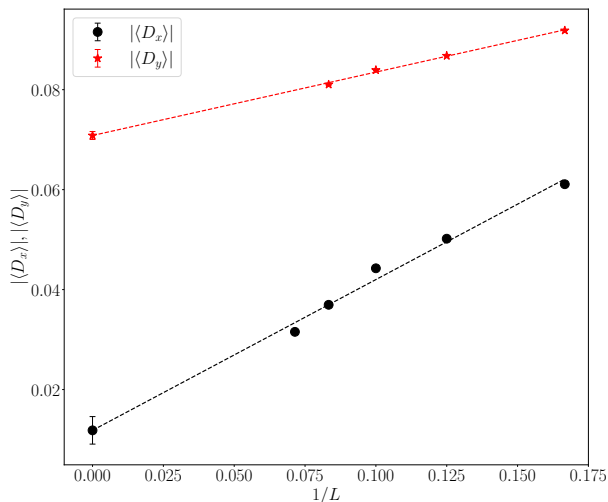


FIG. 6: The VBS dimer order parameter D_α versus $1/L$ for $\Delta_y = 0.03$. The dashed line represents the linear fitting to the data points. For D_x , we use data points from 6×6 to 14×14 , while for D_y , we exclude the data point from the 14×14 system because it is not converged in the FAMPS calculation (details can be found in Appendix. B).

in the J_1 - J_2 square lattice Heisenberg model is a PVBS type.

One may notice that in the extrapolation process to $L \rightarrow \infty$, we utilize data points from the 14×14 system size for D_x but exclude them for D_y (see Fig. 6). The reason for this procedure is as follows. The D_y values obtained from the 14×14 system appear unreasonably high. Moreover, the linear and quadratic extrapolations of D_y with truncation errors in FAMPS give inconsistent values, suggesting a significant finite-bond effect for D_y in the FAMPS calculation. However, the behavior of D_x with truncation errors in FAMPS is quite flat and the extrapolation with truncation errors is robust. More details of the finite-bond effect are discussed in Appendix. B.

In summary, our results indicate that the VBS phase in the J_1 - J_2 square lattice Heisenberg model is a PVBS type.

IV. CONCLUSION

In this work, we employ FAMPS and DMRG methods to the J_1 - J_2 square lattice Heisenberg model to investigate the nature of the VBS phase in its phase diagram. By introducing an anisotropy parameter Δ_y in the nearest neighboring coupling in the y -direction into the system, we are able to distinguish between the CVBS and PVBS types. Through careful extrapolation of truncation errors and employing reliable finite-size scaling, followed by finite Δ_y scaling analysis of the VBS dimer order parameter, we establish that the VBS phase in the J_1 - J_2 square lattice Heisenberg model is a PVBS type, meaning the rotational symmetry is not spontaneously broken in the VBS phase.

Our results not only resolve the long-standing issue on the characterization of the VBS phase in the phase diagram of the J_1 - J_2 square lattice Heisenberg model, but also demonstrate the potential of FAMPS to be applied to other complex two-dimensional systems, where large system sizes and bond dimensions are necessary to capture the intricate details of the ground state.

Acknowledgments

We thank useful discussion with Jong Yeon Lee. The calculation in this work is carried out with TensorKit [49]. We acknowledge the support from the Innovation Program for Quantum Science and Technology (2021ZD0301902), the National Natural Science Foundation of China (Grant No. 12274290) and the sponsorship from Yangyang Development Fund.

-
- [1] E. Dagotto and A. Moreo, Phys. Rev. Lett. **63**, 2148 (1989).
 - [2] S.-S. Gong, W. Zhu, D. N. Sheng, O. I. Motrunich, and M. P. A. Fisher, Phys. Rev. Lett. **113**, 027201 (2014).
 - [3] L. Capriotti, F. Becca, A. Parola, and S. Sorella, Phys. Rev. Lett. **87**, 097201 (2001).
 - [4] N. Read and S. Sachdev, Phys. Rev. Lett. **66**, 1773 (1991).
 - [5] P. W. Anderson, Science **235**, 1196 (1987).
 - [6] X. G. Wen, F. Wilczek, and A. Zee, Phys. Rev. B **39**, 11413 (1989).
 - [7] P. A. Lee, N. Nagaosa, and X.-G. Wen, Rev. Mod. Phys. **78**, 17 (2006).
 - [8] A. W. Sandvik, Phys. Rev. B **56**, 11678 (1997).
 - [9] S. Morita, R. Kaneko, and M. Imada, Journal of the Physical Society of Japan **84**, 024720 (2015).
 - [10] F. Figueirido, A. Karlhede, S. Kivelson, S. Sondhi, M. Rocek, and D. S. Rokhsar, Phys. Rev. B **41**, 4619 (1990).
 - [11] D. Poilblanc, E. Gagliano, S. Bacci, and E. Dagotto, Phys. Rev. B **43**, 10970 (1991).
 - [12] H.J. Schulz, T.A.L. Ziman, and D. Poilblanc, J. Phys. I France **6**, 675 (1996).
 - [13] M. Mambrini, A. M. Läuchli, D. Poilblanc, D. Poilblanc, and F. Mila, Physical Review B **74**, 144422 (2006).
 - [14] J. Oitmaa and Z. Weihong, Phys. Rev. B **54**, 3022 (1996).
 - [15] R. R. P. Singh, Z. Weihong, C. J. Hamer, and J. Oitmaa, Phys. Rev. B **60**, 7278 (1999).
 - [16] J. Sirker, Z. Weihong, O. P. Sushkov, and J. Oitmaa, Phys. Rev. B **73**, 184420 (2006).
 - [17] W.-J. Hu, F. Becca, A. Parola, and S. Sorella, Phys. Rev. B **88**, 060402 (2013).
 - [18] F. Ferrari and F. Becca, Phys. Rev. B **102**, 014417 (2020).

- [19] H.-C. Jiang, H. Yao, and L. Balents, *Phys. Rev. B* **86**, 024424 (2012).
- [20] L. Wang and A. W. Sandvik, *Phys. Rev. Lett.* **121**, 107202 (2018).
- [21] R. Haghshenas and D. N. Sheng, *Phys. Rev. B* **97**, 174408 (2018).
- [22] J. Hasik, D. Poilblanc, and F. Becca, *SciPost Phys.* **10**, 012 (2021).
- [23] W.-Y. Liu, S.-S. Gong, Y.-B. Li, D. Poilblanc, W.-Q. Chen, and Z.-C. Gu, *Science Bulletin* **67**, 1034 (2022).
- [24] Y. Nomura and M. Imada, *Phys. Rev. X* **11**, 031034 (2021).
- [25] D. Poilblanc and M. Mambrini, *Phys. Rev. B* **96**, 014414 (2017).
- [26] L. Capriotti and S. Sorella, *Phys. Rev. Lett.* **84**, 3173 (2000).
- [27] K. Takano, Y. Kito, Y. Ōno, and K. Sano, *Phys. Rev. Lett.* **91**, 197202 (2003).
- [28] M. Mambrini, A. Läuchli, D. Poilblanc, and F. Mila, *Phys. Rev. B* **74**, 144422 (2006).
- [29] R. Darradi, O. Derzhko, R. Zinke, J. Schulenburg, S. E. Krüger, and J. Richter, *Phys. Rev. B* **78**, 214415 (2008).
- [30] J.-F. Yu and Y.-J. Kao, *Phys. Rev. B* **85**, 094407 (2012).
- [31] R. L. Doretto, *Phys. Rev. B* **89**, 104415 (2014).
- [32] H. J. Schulz and T. A. L. Ziman, *Europhysics Letters* **18**, 355 (1992).
- [33] G.-M. Zhang, H. Hu, and L. Yu, *Phys. Rev. Lett.* **91**, 067201 (2003).
- [34] L. Wang, D. Poilblanc, Z.-C. Gu, X.-G. Wen, and F. Verstraete, *Phys. Rev. Lett.* **111**, 037202 (2013).
- [35] W.-Y. Liu, S. Dong, C. Wang, Y. Han, H. An, G.-C. Guo, and L. He, *Phys. Rev. B* **98**, 241109 (2018).
- [36] X. Qian and M. Qin, *Chinese Physics Letters* **40**, 057102 (2023).
- [37] X. Qian and M. Qin, *Phys. Rev. B* **109**, L161103 (2024).
- [38] S. R. White, *Phys. Rev. Lett.* **69**, 2863 (1992).
- [39] S. R. White, *Phys. Rev. B* **48**, 10345 (1993).
- [40] U. Schollwöck, *Rev. Mod. Phys.* **77**, 259 (2005).
- [41] S. Östlund and S. Rommer, *Phys. Rev. Lett.* **75**, 3537 (1995).
- [42] F. Verstraete and J. I. Cirac, *Phys. Rev. B* **73**, 094423 (2006).
- [43] V. M. F. Verstraete and J. Cirac, *Advances in Physics* **57**, 143 (2008).
- [44] J. Eisert, M. Cramer, and M. B. Plenio, *Rev. Mod. Phys.* **82**, 277 (2010).
- [45] G. Vidal, *Phys. Rev. Lett.* **101**, 110501 (2008).
- [46] T. Felser, S. Notarnicola, and S. Montangero, *Phys. Rev. Lett.* **126**, 170603 (2021).
- [47] X. Qian and M. Qin, *Phys. Rev. B* **105**, 205102 (2022).
- [48] B. Zhao, J. Takahashi, and A. W. Sandvik, *Phys. Rev. B* **101**, 157101 (2020).
- [49] The code is developed with TensorKit package at <https://github.com/Jutho/TensorKit.jl>.

Appendix A: Finite-size scaling

In Fig. 7, we show the extrapolation of the VBS dimer order parameter with respect to the system sizes at $\Delta_y = 0.01, 0.02, 0.05$, and 0.07 .

Appendix B: Finite-bond effect of FAMPS results for the 14×14 system

To elucidate the finite-bond effect on the VBS dimer order parameter, particularly the unreliability of the results for D_y at system size 14×14 , we present the extrapolation of the VBS dimer order parameter with respect to the truncation errors in FAMPS calculations for the system with size 14×14 in Fig. 8. For both D_x and D_y , linear and quadratic fittings are employed to extrapolate the truncation errors to $\varepsilon = 0$. Notably, both fittings give consistent results for D_x . However, for D_y , linear and quadratic fittings give different results.

Due to the computational resource limitation, achieving the required bond dimension for the convergence of D_y in the 14×14 system size is challenging. So we exclude the data for size 14×14 when performing the finite-size scalings for D_y .

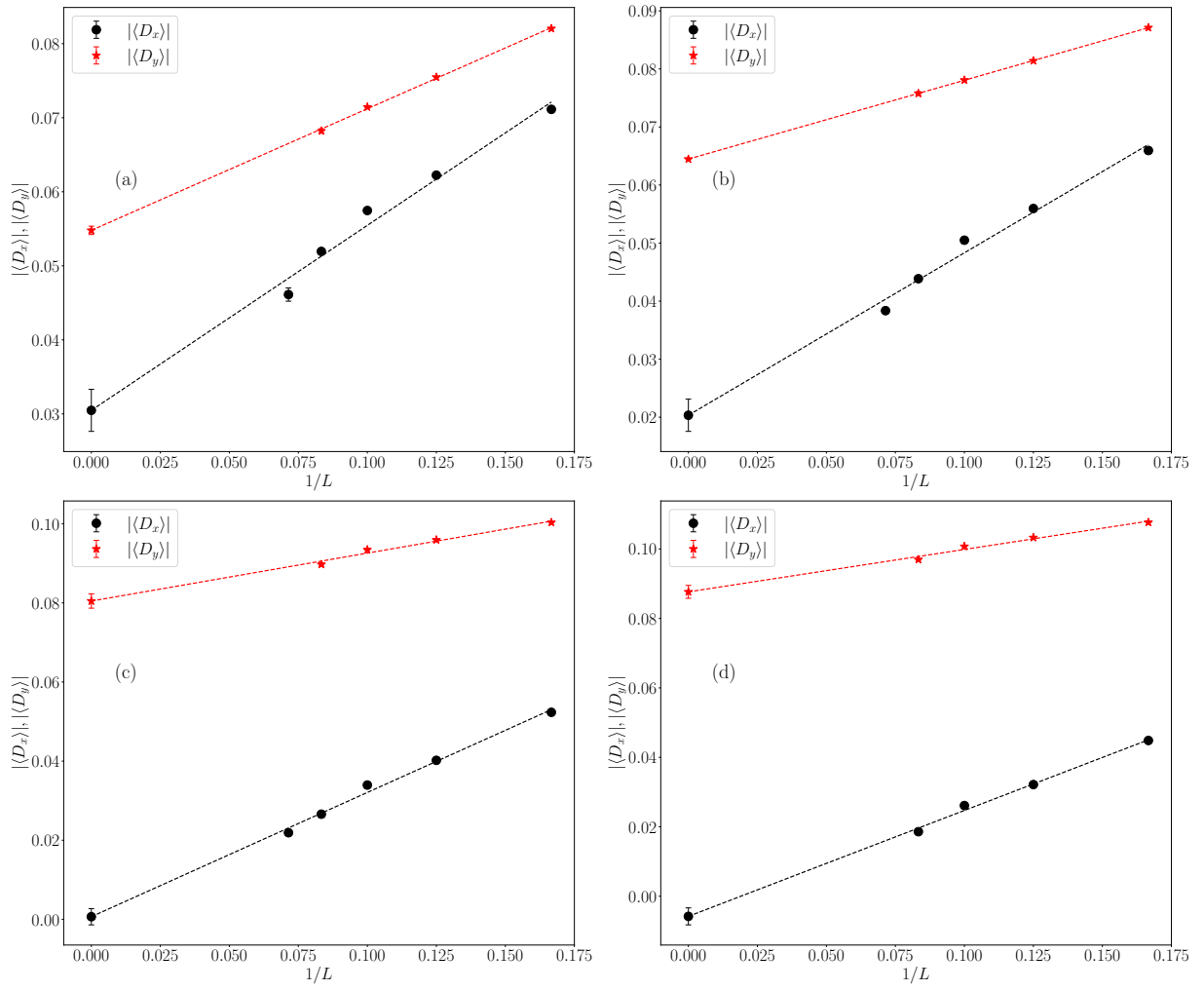


FIG. 7: VBS dimer order parameter D_α plotted as a function of system size $1/L$. The dashed line represents a linear fitting to the data points. (a) results for $\Delta_y = 0.01$, (b) results for $\Delta_y = 0.02$, (c) results for $\Delta_y = 0.05$, and (d) results for $\Delta_y = 0.07$.

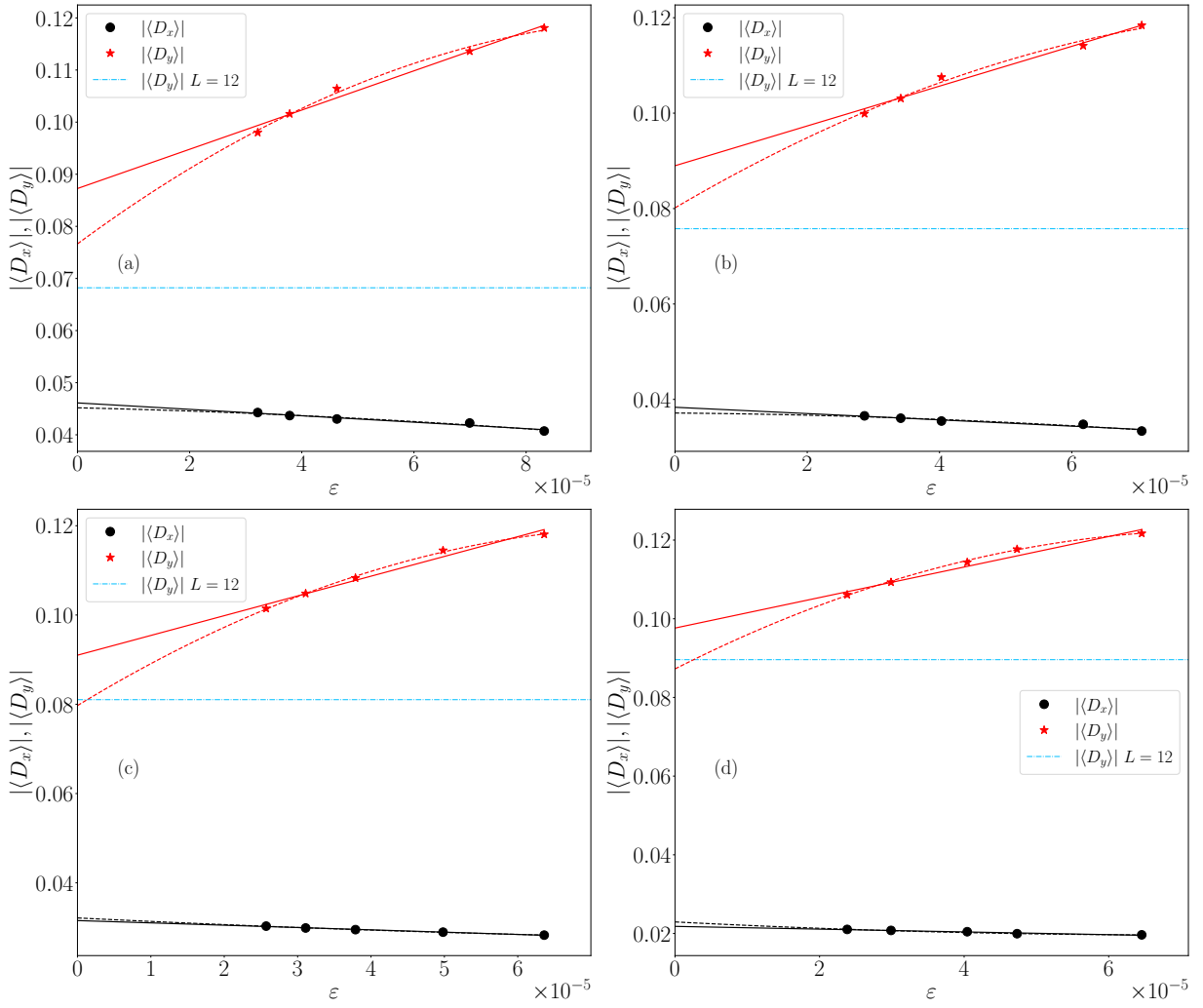


FIG. 8: VBS dimer order parameter D_α plotted as a function of truncation errors ϵ for the 14×14 system. The solid line indicates a linear fitting to the data points, while the dashed line represents a quadratic fitting. The blue dot-dash line represents the extrapolated value of D_y for the 12×12 system as a reference. (a) $\Delta_y = 0.01$, (b) $\Delta_y = 0.02$, (c) $\Delta_y = 0.03$ and (d) $\Delta_y = 0.05$. We can find that the extrapolation for D_x is robust, whereas it is not reliable for D_y .